tion energy should be smaller than ΔE_J as the kinetic energy is expected to increase below the superconducting state. Taking this into account, we see that the spectral weight of the π resonance peak can quantitatively account for the condensation energy measured from H_c and specific-heat experiments, in reasonable agreement with the prediction based on our mechanism.

We now compare our mechanism for HTSC with the spin fluctuation pairing mechanism[23–25]. All these mechanisms are based on the antiferromagnetic exchange interaction interaction E_J. Our analysis of the neutron data confirms that a large part of the condensation energy indeed arises from such an exchange interaction[8]. However, our mechanism differs from the spin fluctuation pairing mechanism, both conceptually and quantitatively. The idea of spin fluctuation pairing is directly borrowed from the phonon-mediated pairing in the traditional BCS superconductors. It requires sizeable antiferromagnetic spin fluctuations in the normal state, in order to pair the Fermi liquid like quasiparticles. In contrast, in our mechanism, the antiferromagnetic spin fluctuations in the normal state do not play an important role in driving superconductivity. In the superconducting state, the π resonance can be viewed as a kind of spin fluctuation in a particular frequency and momentum range. From the point of view of the $SO(5)$ theory[13], the superconducting state is obtained from the antiferromagnetic state by a rotation, so it is natural to expect it to have more antiferromagnetic correlation than the normal state. The crucial conceptual difference between these two mechanisms therefore lies in the fact that normal state antiferromagnetic spin fluctuations are not required in our mechanism. This conceptual difference has a direct quantitative consequence. From equation (4), we see that the presence of spin fluctuation spectral weight in the normal state contributes negatively to the condensation energy. It is not clear why the spin fluctuation model would predict a change in the frequency-integrated weight of $S(q,\omega)$ near $q = Q$. In fact, most theories of the neutron resonance peak based on the spin fluctuation models[26,27] assume a pre-existing overdamped spin fluctuation mode in the normal state and only predict a reduction of damping below T_c with essentially conserved weight.

Our mechanism provides a natural explanation for the doping dependence of the condensation energy. We attribute the condensation energy to the difference in exchange energies in superconducting and normal states. More-underdoped materials have considerably more antiferromagnetic correlations in the normal state, as known from neutron scattering[28]. Although in the superconducting state the weight of the resonance is enhanced[29], the difference between the normal and the superconducting exchange energies becomes smaller. This is consistent with the results of Loram *et al.*[30] who find a decrease in the condensation energy with decreased doping in $Y_{0.8}Ca_{0.2}Ba_2Cu_3O_{6+x}$. Until this point we have been discussing the relation between the condensation energy and the resonant peaks in neutron scattering at zero temperature. It would be interesting to see whether this idea also works at finite temperature. Without going into details, we would like to point out a striking similarity between the temperature dependence of H_c (ref. 2) and that of the resonance intensity[29,31] for the underdoped copper oxides: both quantities scale similarly below T_c and both have 'tails' extending above T_c, presumably arising from significant pairing fluctuations in the pseudogap regime. These phenomena await future investigations. □

Received 4 June; accepted 16 September 1998.

1. Shrieffer, J. R. *Theory of Superconductivity* (Addison-Wesley, Reading, MA, 1964).
2. Loram, J. *et al.* The electronic specific heat of $YBa_2(Cu_{1-x}Zn_x)_3O_7$ from 1.6 to 300 K. *Physica C* **171,** 243–256 (1990).
3. Loram, J. *et al.* Electronic specific heat of $YBa_2Cu_3O_{6+x}$ *et al.* from 1.8 to 300 K. *J. Supercond.* **7,** 243–249 (1994).
4. Chester, G. V. Difference between normal and superconducting states of a metal. *Phys. Rev.* **103,** 1693–1699 (1956).
5. Chakravarty, S. *et al.* Interlayer tunneling and gap anisotropy in high temperature superconductors. *Science* **261,** 337–340 (1993).
6. Leggett, A. Where is the energy saved in cuprate superconductivity? Preprint, Univ. Illinois at Urbana-Champaign (1998).
7. Zhang, F. C. & Rice, T. M. Effective Hamiltonian for the superconducting copper-oxides. *Phys. Rev. B* **37,** 3759–3763 (1988).
8. Scalapino, D. J. & White, S. The superconducting condensation energy and an antiferromagnetic exchange based pairing mechanism. Preprint cond-mat/9805075 at ⟨http://xxx.lanl.com⟩ (1998).
9. Demler, E. & Zhang, S. C. Theory of resonance neutron scattering of high T_c superconductors. *Phys. Rev. Lett.* **76,** 4126–4129 (1995).
10. Meixner, S. *et al.* Finite size studies on the $SO(5)$ symmetry of Hubbard model. *Phys. Rev. Lett.* **79,** 4902–4905 (1997).
11. Eder, R., Hanke, W. & Zhang, S. C. Numerical evidence for $SO(5)$ symmetry and superspin multiplets in the two dimensional t-J model. *Phys. Rev. B* **57,** 13781–13789 (1998).
12. Demler, E., Kohno, H. & Zhang, S. C. π excitation of the t-J model. *Phys. Rev. B* **58,** 5719–5730 (1998).
13. Zhang, S. C. A unified theory based on $SO(5)$ symmetry of superconductivity and antiferromagnetism. *Science* **275,** 1089–1096 (1997).
14. Mook, H. *et al.* Polarized neutron determination of the magnetic excitation in $YBa_2Cu_3O_7$. *Phys. Rev. Lett.* **70,** 3490–3493 (1993).
15. Fong, H. F. *et al.* Phonon and magnetic neutron scattering at 41 meV in $YBa_2Cu_3O_7$. *Phys. Rev. Lett.* **75,** 316–319 (1995).
16. Fong, H. F. *et al.* Polarized and unpolarized neutron scattering study of the dynamic spin susceptibility in $Yba_2Cu_3O_7$. *Phys. Rev. B* **54,** 6708–6720 (1996).
17. Shastry, S. & Sutherland, B. Twisted boundary conditions and effective mass in Heisenberg-Ising and Hubbard rings. *Phys. Rev. Lett.* **65,** 243–246 (1990).
18. Scalapino, D., White, S. & Zhang, S. C. Superfluid density and the Drude weight of the Hubbard model. *Phys. Rev. Lett.* **68,** 2830–2833 (1992).
19. Chakravarty, S. Do electrons change their c-axis kinetic energy upon entering the superconducting state? Preprint cond-mat/9801025 at ⟨http://xxx.lanl.gov⟩ (1998).
20. Timusk, T. & Statt, B. The pseudogap in high temperature superconductors: an experimental survey. *Rep. Prog. Phys.* (in the press).
21. Reznik, D. *et al.* Direct observation of optical magnons in $YBa_2Cu_3O_{6.2}$. *Phys. Rev. B* **53,** R14741–R14744 (1996).
22. Hayden, S. *et al.* High frequency spin waves in $YBa_2Cu_3O_{6.15}$. *Phys. Rev. B* **54,** R6905–R6908 (1996).
23. Scalapino, D. The case for $d_{x^2-y^2}$ pairing in the cuprate superconductors. *Phys. Rep.* **250,** 329–365(1995).
24. Pines, D. Understanding high-temperature superconductivity, a progress report. *Physica B* **199–200,** 300–309 (1994).
25. Shrieffer, J. R. Ward's identity and the suppression of spin fluctuation superconductivity. *J. Low Temp. Phys.* **99,** 397–402 (1995).
26. Bulut, N. & Scalapino, D. Neutron scattering from a collective spin fluctuation mode in CuO_2 bilayer. *Phys. Rev. B* **53,** 5149–5152 (1996).
27. Morr, D. K. & Pines, D. The resonance peak in cuprate superconductors. Preprint cond-mat/9805107 at ⟨http://xxx.lanl.gov⟩ (1998).
28. Hayden, S. *et al.* Absolute measurements of the high-frequency magnetic dynamics in high-Tc superconductors. *Physica B* **241–243,** 765–772 (1998).
29. Fong, H. F. *et al.* Superconductivity-induced anomalies in the spin excitation spectra of underdoped $YBa_2Cu_3O_{6+x}$. *Phys. Rev. Lett.* **78,** 713–716 (1997).
30. Loram, J. W. *et al.* Superconducting and normal state energy gaps in $Y_{0.8}Ca_{0.2}Ba_2Cu_3O_{7-\delta}$ from the electronic specific specific heat. *Physica C* **282–287,** 1405–1406 (1997).
31. Dai, P. *et al.* Magnetic dynamics in underdoped $YBa_2Cu_3O_{7-x}$: direct observation of a superconducting gap. *Phys. Rev. Lett.* **77,** 5425–5428 (1996).

Acknowledgements. We thank P. Dai, H. Fong, S. Heyden, B. Keimer, H. Mook and D. Scalapino for discussions.

Correspondence and requests for materials should be addressed to E.D. (e-mail: demler@itp.ucsb.edu).

Moisture-induced ageing in granular media and the kinetics of capillary condensation

L. Bocquet*, E. Charlaix*†, S. Ciliberto* & J. Crassous*

* *Laboratoire de Physique de l'ENS de Lyon (URA CNRS 1325), 46 Allée d'Italie, 69364 Lyon Cedex, France*

† *DPM (UMR CNRS 5586), Université Claude Bernard-Lyon I, 43 Boulevard du 11 Novembre 1918, 69622 Villeurbanne Cedex, France*

In 1773 Coulomb[1] recognized that the static properties of granular systems can be discussed in terms of the frictional properties between different layers[2], leading to his relationship between the angle of repose of a granular pile (θ_0) and the coefficient of static friction μ_s: $\tan\theta_0 = \mu_s$. Two centuries later, solid friction and granular media still present many puzzles. One such is that the coefficient of static friction depends on the time during which the solids remain in contact before the measurement. Here we show that this ageing effect is manifested too in the angle of repose of granular media and originates from capillary condensation of water vapour between the packed particles, leading to the formation of water bridges. By assuming that the kinetics of this process are governed by the thermally activated nucleation of bridges, we can reproduce both the time- and humidity-dependence of the ageing behaviour. Our results also clarify the kinetics of adsorption in porous media more generally.

Ageing is said to occur in systems for which the relaxation time becomes so long that it may not reach equilibrium on a laboratory timescale (typically hours). The measured properties of such a system therefore depend on the time at which the measurement is made. This is the case for solid friction: the friction coefficient depends on the time elapsed after the surfaces have come into contact[3–5]. This dependence of μ_s on waiting time is observed with almost all materials (from paper to rocks) and is found universally to be logarithmic. Although solid friction is related to the properties of granular media, as emphasized by Coulomb's analogy, ageing in granular media has previously received little attention.

We have studied the effect of waiting time on the angle of first avalanche θ_w of a granular system of small (typically 200-μm) spherical glass beads contained in a rotating drum (Fig. 1a). We observe logarithmic ageing of the maximum static angle θ_w (Fig. 2a). This logarithmic behaviour spans more than three orders of magnitude in time, ranging from 5 seconds to more than 2 hours. Ageing was not observed for beads with a diameter larger than 0.5 mm, except at very large humidities. It is known that humidity can exert an important influence on granular media[2]. Addition of small quantities of wetting liquid has been shown to change enormously the repose angle of a pile[6,7]; a brief discussion of moisture effects can even be found in Coulomb's treatise[1]. We repeated our experiments at various humidities P_v/P_{sat} (P_v and P_{sat} being respectively the vapour pressure and saturated water pressure), and found humidity to be the crucial parameter controlling the ageing of θ_w: no ageing is observed at low humidity, and the magnitude of the ageing effect increases dramatically with humidity (Fig. 2b).

This humidity dependence leads to the intuitive idea that the ageing effect originates from the condensation of small liquid bridges between the beads. Liquid bridges induce a significant cohesion between the beads, which can increase the friction between different layers of the granular system and result in a higher value of θ_w. However, the physical justification for such

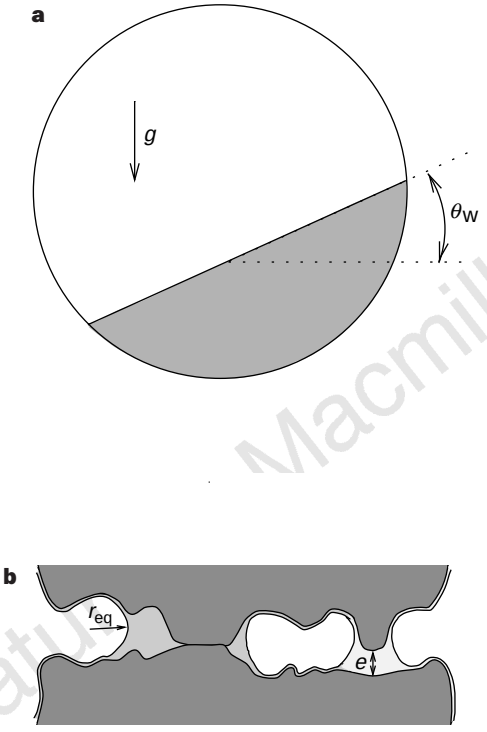

Figure 1 Experimental set-up. **a**, Principle of the experimental setup. Glass beads fill 25% of the volume of a cylinder (diameter 100 nm, length 13 mm) which can rotate around its axis. Two systems were studied; a 'polydisperse' system with 140 μm < d < 260 μm, and a 'monodisperse' system with 200 μm < d < 250 μm, where d is the diameter of the beads. The walls of the cylinder are glass, and the shape of the pile of beads is recorded with a video camera. Experiments are performed at room temperature, under controlled humidity (defined as the ratio between the vapour pressure and saturated pressure of water, P_v/P_{sat}). Before starting experiments, the system is prepared by rotating the drum for ~12 h. Then the ageing properties are investigated for various values of P_v/P_{sat} using the following protocol: first, the system is put in motion for a few turns (typically three); second, the end of this 'motion period' defines the origin of waiting time $t_w = 0$, after which the system is left at rest; third, after a given time (ranging from 10 to 10^4 s), a slow rotational motion (<1 turn per min) is transmitted to the cylindrical drum. The angle θ_w at which the first avalanche takes place is measured from the slope of the beads just before the avalanche. The same procedure is repeated for different waiting times t_w and a curve of θ_w versus waiting time t_w is constructed. **b**, Schematic drawing of the contact at the nanometre scale between two micrometre-size asperities on the beads. Inside most of the contact region, the solid surfaces do not touch each other at the molecular scale, and capillary condensation occurs in the gap left between the surfaces.

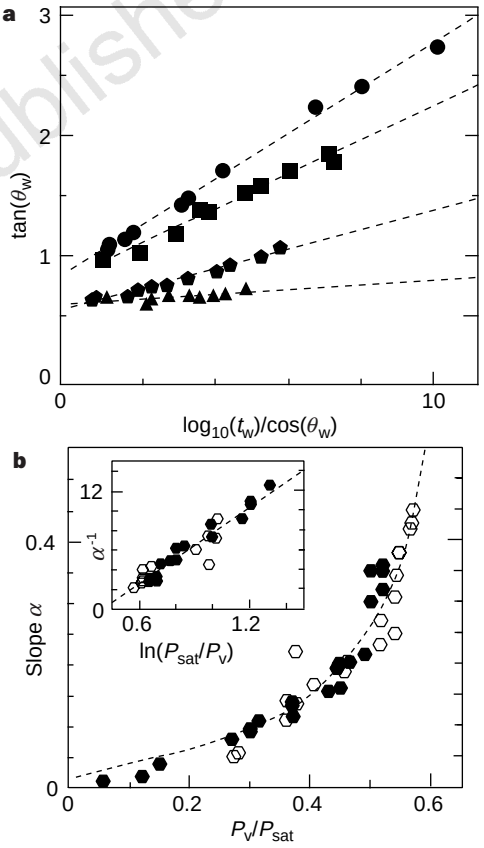

Figure 2 Dependence of ageing on humidity. **a**, Logarithmic ageing of the angle of first avalanche. The ageing property is analysed by plotting $\tan\theta_w(t_w)$ as a function of $\log_{10}(t_w)/\cos\theta_w(t_w)$, for different values of the water vapour pressure P_v (see equation (3)). The time is in units of seconds. From bottom to top, humidity is: 15% (triangles), 27% (pentagons), 36.1% (squares) and 45.5% (circles). In these measurements, times range typically over nearly four orders of magnitude. The dotted lines are least-square fits of the experimental data, whose slope is $\alpha(P_v)$. **b**, Variation of the slope $\alpha(P_v)$ characterizing the ageing behaviour of the first avalanche angle (see equation (3)) with humidity P_v/P_{sat}. Open symbols, the polydisperse system; filled symbols, the monodisperse system. The dashed line is the theoretical prediction $\alpha = \alpha_0/\ln(P^*_{sat}/P_v)$, where $\alpha_0 = 0.079$ and $P^*_{sat} = 0.68P_{sat}$. The validity of the previous theoretical prediction is best confirmed by the measured linear dependence of $1/\alpha$ as a function of $\ln(P_{sat}/P_v)$ (see inset): in this plot, a linear least-squares fit thus provides unambiguously values of α_0 and P^*_{sat}. The lowering observed in the saturating pressure P^*_{sat} might be an effect of the long-range attractive forces exerted by the walls, and/or of dissolved species in the condensed water.

behaviour is not so obvious. We consider first the idealized situation of two smooth beads in contact. The capillary adhesion force exerted by a small liquid bridge connecting the beads is given by the product of the liquid surface tension γ and the radius of the beads (we note that if solid deformation occurs, the numerical prefactor changes slightly[8]): $F_{adh} \approx 2\pi\gamma R$, regardless of the size of the (small) bridge[9]. Therefore, the adhesion force has no humidity-dependence, and moreover would be able to stick all the beads together[2]. This apparent difficulty disappears if one takes into account the roughness of the beads. The spatial extent of a liquid bridge is controlled by the radius of curvature r_{eq} of the liquid interface, which, at liquid–vapour equilibrium, is fixed by the Kelvin relation[10]

$$\frac{\gamma}{r_{eq}} = \rho_l k_B T \ln\frac{P_{sat}}{P_v} \equiv \rho_l \Delta\mu \quad (1)$$

where ρ_l is the density of the liquid and $\Delta\mu = k_B T \ln(P_{sat}/P_v)$ is the undersaturation of the chemical potential. Under ambient conditions, this yields a value of r_{eq} of nanometre dimensions. A crucial consequence is that liquid bridges are able to form only in nanometre-scale interstices. Because the beads are not smooth at the nanometre scale, the wetted region does not spread over the whole area it would occupy if the beads were smooth, and the cohesive force is reduced in proportion. We also note the slow evolution in time of the cohesive properties, measured through the time-dependence of θ_w. This indicates that the condensation of liquid bridges takes place over long timescales. However, surface-force experiments on capillary condensation between smooth surfaces separated by a gap show clearly that the condensation of a liquid bridge occurs from a metastable state; that is, a metastable vapour phase can stay for a long time (of the order of several minutes) between the surfaces, whereas the equilibrium state is a liquid bridge[11,12].

On the basis of these considerations, we propose a model for the ageing behaviour based on the hypothesis that capillary condensation arises through an activated process. This assumption is justified by the first-order character of capillary condensation. We consider two surfaces separated by a gap, and in contact with undersaturated vapour. A thin wetting film coats both surfaces. For gaps of less than a critical distance, of the order of the Kelvin radius r_{eq}, this state is metastable[10]: capillary condensation should occur. However, an energy barrier has to be overcome, as the coating films have to grow and coalesce in order to fill the gap between the surfaces. Along this path, the free energy of the system increases to a maximum as the films are about to merge[11]. The energy barrier, ΔE, is therefore the free energy cost of condensing the corresponding water volume from the undersaturated vapour phase: $\Delta E \approx \Delta\mu\rho_l v_l$, where v_l is the liquid volume needed to nucleate the liquid bridge. In the case of two rough beads, nucleation occurs preferentially between the asperities and the nucleation volume is $v_l = a_0^2 e$, where e is the gap between the surfaces at the nucleating site and a_0^2 is a typical nucleation area (Fig. 1b). A more sophisticated model taking the long-range forces into account confirms this estimation.

Assuming an activation process, the time τ needed to condense a liquid bridge in an interstitial volume is $\tau \approx \tau_0 \exp(\Delta E/k_B T)$, with τ_0 being a microscopic time. Typically, τ_0 is of the order of the time needed to condense one liquid layer. Because both beads are rough, many liquid bridges can form in the macroscopic contact region. One expects, moreover, that the nucleating sites will exhibit a broad distribution of gaps e between solid surfaces, and that the activation times are accordingly widely distributed. After a given time t_w, only the bridges with an activation time τ_{act} smaller than t_w have condensed. These were therefore formed at the nucleating sites with a gap e, verifying that $e < e_{max}(t_w) = (k_B T/\Delta\mu)(\rho_l a_0^2)^{-1} \ln(t_w/\tau_0)$. Once a liquid bridge has condensed, it fills locally the volume surrounding the nucleating site, until the Kelvin equilibrium condition for the radius of curvature, equation (1), is met. Thus because of roughness, only a fraction $f(t_w)$ of the total wettable area is indeed wetted at a given time t_w. This fraction $f(t_w)$ is proportional to the number of activated bridges, yielding (to a first approximation) $f(t_w) \approx e_{max}(t_w)/\lambda$, where λ is the typical width of the distribution of distances between the surfaces. The capillary adhesion force is proportional to the wetted area and is thus reduced by the factor $f(t_w)$ from the perfectly smooth case ($F_{adh} \approx 2\pi\gamma R$), leading to

$$F_{adh}(t_w) \approx \gamma\, d \frac{1}{\ln(P_{sat}/P_v)} \ln\left(\frac{t_w}{\tau_0}\right) \quad (2)$$

where $d = 2\pi R/(\lambda\rho_l a_0^2)$ is a distance taking into account the geometrical characteristics of the contact. By reproducing Coulomb's argument for the stability of the surface layer in the presence of this additional adhesive force[1,7], we obtain the following equation for $\theta_w(t_w)$:

$$\tan\theta_w(t_w) \approx \tan\theta_0 + \frac{\alpha(P_v)}{\cos\theta_w(t_w)} \log\left(\frac{t_w}{t_0}\right) \quad (3)$$

where $\alpha(P_v) = \alpha_0/\ln(P_{sat}/P_v)$. Here α_0 is a dimensionless parameter taking into account the relative strength of the adhesion force and the weight of the material. Thus, by plotting $\tan\theta_w(t_w)$ as a function of $\log(t_w)/\cos\theta_w(t_w)$, one should obtain a straight line. This expectation is indeed borne out experimentally (Fig. 2a). Moreover, the increase in the slope, $\alpha(P_v)$, of this line with humidity is in good agreement with the theoretical prediction of equation (3) (Fig. 2b). Our model is thus able to reproduce both the waiting-time- and humidity-dependence of the measured ageing properties of a granular system.

Our results highlight the crucial role of humidity in the statics of granular systems. The similarity between ageing in granular media and ageing of the static friction coefficient in dry friction is reflected in the reported effect of humidity on the friction between rocks[4]; in that study, the 'standard' ageing properties of μ_s were similarly found to disappear at zero humidity. Similar behaviour has also been observed in indentation experiments[13]. The mechanism previously suggested to explain ageing behaviour in solid friction involves asperity creep[14]; our work suggests that humidity-induced capillary condensation may provide an alternative explanation for this effect. □

Received 26 January; accepted 2 September 1998.

1. Coulomb, C. A. Sur une application des règles de Maximis et Minimis à quelques Problèmes de Statique, relatifs à l'Architecture, in *Mémoires de Mathématiques et de Physique, Académie Royale des Sciences, Paris*, 343–382 (1773).
2. Duran, J. *Sables, Poudres et Grains* (Eyrolles Sciences, Paris, 1997).
3. Scholz, C. H. *The Mechanics of Earthquakes and Faulting* (Cambridge Univ. Press, 1990).
4. Dieterich, J. & Conrad, G. Effect of humidity on time- and velocity-dependent friction in rocks. *J. Geophys. Res.* **89,** 4196–4202 (1984).
5. Heslot, F., Baumberger, T., Perrin, B., Caroli, B. & Caroli, C. Creep, stick-slip, and dry-friction dynamics: Experiments and a heuristic model. *Phys. Rev. E* **49,** 4973–4988 (1994).
6. Hornbaker, D. J., Albert, R., Albert, I., Barabasi, A.-L. & Schiffer, P. What keeps sandcastles standing? *Nature* **387,** 765 (1997).
7. Halsey, T. C. & Levine, A. J. How sandcastles fall. *Phys. Rev. Lett.* **80,** 3141–3144 (1998).
8. Maugis, D. Adhesion of spheres: the JKR-DMT transition using a Dugdale model. *J. Colloid Interface Sci.* **150,** 243–269 (1992).
9. Israelachvili, J. N. *Intermolecular and Surfaces Forces* (Academic, London, 1985).
10. Evans, R. in *Liquids at Interfaces* (eds Charvolin, J., Joanny, J. F. & Zinn-Justin, J.) 3–98 (Elsevier Science, New York, 1989).
11. Crassous, J., Charlaix, E. & Loubet, J.-L. Capillary condensation between high-energy surfaces. An experimental study with a surface force apparatus. *Europhys. Lett.* **28,** 37–42 (1994).
12. Iwamatsu, I. & Horii, K. Capillary condensation and adhesion of two wetted surfaces. *J. Colloid Interface Sci.* **182,** 400–406 (1996).
13. Westbrook, J. H. & Jorgensen, P. J. Effect of water desorption on indentation microhardness anisotropy in minerals. *Am. Mineral.* **53,** 1899–1914 (1968).
14. Estrin, Y. & Brechet, Y. On a model of frictional sliding. *Pure Appl. Geophys.* **147,** 745–762 (1996).

Acknowledgements. We thank J.-M. Georges and M.L. Bocquet for discussions. L.B. thanks J. Duran for providing ref. 1.

Correspondence and requests for materials should be addressed to L.B. (e-mail: lbocquet@physique.ens-lyon.fr).